High-Efficiency Octave Bandwidth Rectifier for Electromagnetic Energy Harvesting

Haoming He, *Graduate Student Member, IEEE*, Yilin Zhou, Zhongqi He, Yuhao Feng, and Changjun Liu, *Senior Member, IEEE*

***Abstract*— This letter presents the design and implementation of a compact high-efficiency octave microwave rectifier. A key highlight is the novel segmented impedance matching method, a unique approach that expands the rectifier bandwidth. The diode reactance is initially regulated by a series short-ended microstrip line. Impedance-compensated structures, characterized by varying admittance properties across an extensive frequency range, partition the operating frequency band into two segments based on the input impedance, thereby minimizing impedance variation. Ultimately, the input impedance is matched by a novel triple-band matching network. An octave rectifier was fabricated and measured. Results demonstrate that the rectifier achieves over 50% efficiency over 1.3–2.55 GHz (fractional bandwidth 64.9%) at 0-dBm RF input power. Even with a decrease in input power to −10 dBm, the rectifier maintains over 30% efficiency.**

***Index Terms*— Broadband, energy harvesting, high efficiency, impedance match, rectifier.**

I. Introduction

Energy harvesting, as one of the new technologies, has a very promising application prospects [1], [2], [3]. Electromagnetic energy harvesting enables the construction of self-powered or near-self-powered systems, which are critical for applications, such as the Internet-of-Things devices [4], [5], wireless sensor networks [6], [7], [8], and communication nodes in remote areas. Broadband high-efficiency rectifiers that can be applied at low power are the focus of research for better harvesting of electromagnetic energy in space.

Several proposals have been suggested to enhance the operational efficiency of the rectifiers. Nonuniform transmission lines are used for impedance matching of wideband rectifiers to achieve high rectification efficiency [9], [10]. On the other hand, the rectifiers using harmonic controlling circuits have been successfully enhanced, expanding the bandwidth without increasing the size [11], [12]. In terms of novel impedance compression techniques, the primary method to achieve small size and high efficiency is to compress the variation range of the rectifier input impedance [13], [14], [15], [16], [17]. Using voltage-doubling circuits combined with broadband matching networks, such as simplified real-frequency techniques [18], [19], [20] and two-branch impedance matching circuits [21], can help make rectifiers compact and efficient.

This letter introduces an innovative octave rectifier with high efficiency for energy harvesting applications. The design includes impedance adjustment, compensation, and matching, which divides the rectifier's working frequency band into two segments: real impedance matching and complex impedance matching, improving both efficiency and operating bandwidth. We analyze the matching network and imaginary part compensation and then fabricate and measure an octave rectifier with an operating bandwidth of 1.3–2.55 GHz.

Received 5 August 2024; revised 11 October 2024; accepted 24 November 2024. This work was supported in part by NFSC under Grant U22A2015 and Grant 62071316. *(Corresponding author: Changjun Liu.)*

Haoming He, Yilin Zhou, Zhongqi He, and Changjun Liu are with the School of Electronics and Information Engineering, Sichuan University, Chengdu 610064, China, and also with Yibin Industrial Technology Research Institute of Sichuan University, Yibin 644000, China (e-mail: cjliu@ieee.org).

Yuhao Feng is with the School of Electronic Science and Engineering, University of Electronic Science and Technology of China, Chengdu 610054, China.

Digital Object Identifier 10.1109/LMWT.2024.3510153

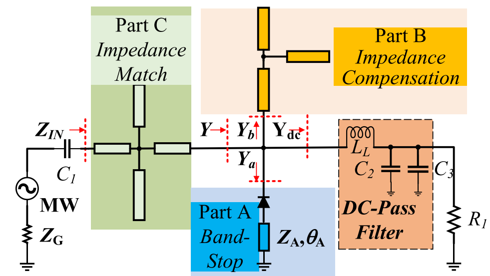

Fig. 1. Schematics of octave rectifier.

II. Principle and Design

Fig. 1 shows the operating principle diagram of the octave rectifier. It has three main parts: Part A adjusts the diode's admittance to Y_a, Part B supplies admittance Y_b to compensate Y_a to Y, and Part C matches the admittance Y to the source. $Y_{\rm dc} = 0$, and $Y = Y_a + Y_b$.

In the design, to enhance the rectifier's bandwidth, the input admittance of the diode is optimized using two segments in its operating band. Define the starting and stopping frequencies of the operating band and the frequencies of the segments as fixed f_1, f_3, f_2, respectively, and $f_1 < f_2 < f_3$. It is required that the admittance of Parts A and B in parallel is complex from f_1 to f_2 and real from f_2 to f_3, which meets the design requirement of segment matching. Part C comprises a cross structure intended for impedance matching. The operating bandwidth of the rectifier is effectively broadened by matching the input impedance of the rectifier in two segments. The electrical lengths are both defined at f_1.

A. Impedance Compensation Structures

The topology of impedance compensation structures is shown in Fig. 2(a). Y_{b1} and Y_{b2} are the input admittances of microstrip lines. We denote $k_2 = f_2/f_1$ and $k_3 = f_3/f_1$.

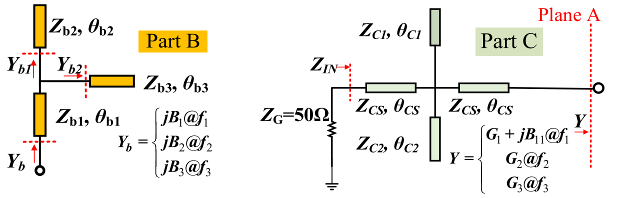

(a) (b)

Fig. 2. (a) Impedance compensation structures. (b) Triple-band matching network.

To simplify the procedure, first, it is satisfied with $Y_{b2} = 0@f_2$, which could be achieved by implementing a quarter-wave open-ended transmission line. Subsequently, upon selecting and fixing the characteristic impedance of Z_{B1}, the electrical length of θ_{b1} is expressed as follows:

$$\theta_{b1} = \frac{1}{k_2}\tan^{-1}\left(\frac{-1}{Z_{b1}B_2}\right). \quad (1)$$

When Z_{b1} and θ_{b1} are calibrated, the admittance at f_1 and f_3 is

$$Y_{b1} + Y_{b2} = \left[\frac{-j(B_1 Z_{b1} + \tan\theta_{b1})}{Z_{b1} + Z_{b1}^2 \tan\theta_{b1}}\right]_{f=f_1} = \left[\frac{-j(B_3 Z_{b1} + \tan(k_3\theta_{b1}))}{Z_{b1} + Z_{b1}^2 B_3 \tan(k_3\theta_{b1})}\right]_{f=f_3}. \quad (2)$$

It also satisfies

$$Y_{b1} + Y_{b2} = \left[\frac{j\tan(\theta_{b2})}{Z_{b2}} + \frac{j\tan(\theta_{b3})}{Z_{b3}}\right]_{f=f_1} = \left[\frac{j\tan(k_3\theta_{b2})}{Z_{b2}} + \frac{j\tan(k_3\theta_{b3})}{Z_{b3}}\right]_{f=f_3}. \quad (3)$$

Solving (3) and (4) in association, the structural parameters of the entire Part B can be calculated.

B. Impedance Match Structure

A novel triple-band matching network is proposed. As depicted in Fig. 2(b), the triple-frequency matching network comprises a cross-shaped microstrip network structure. When working with three frequencies, f_1, f_2, and f_3, it can realize impedance matching at f_2 and f_3 for pure resistance as well as realize impedance matching at f_1 for complex impedance.

A quarter wavelength transmission line is used as the impedance converter in impedance matching. The relationship between input impedance Z_{in} and load impedance Z_L meets

$$Z_{\text{in}} = \frac{Z_0^2}{Z_L} \quad (4)$$

where Z_0 is the transmission line characteristic impedance.

For frequencies f_2 and f_3, the cross circuit is equivalent to a quarter-wave transmission line, so both have the same *ABCD* matrix. *ABCD* matrix for Part C is as follows (5) and (6), as shown at the bottom of the next page, where Z_{CS}, Z_{C1}, Z_{C2}, θ_{CS}, θ_{C1}, and θ_{C2} are the characteristic impedance and electrical length of microstrip lines, as shown in Fig. 2(b).

The *ABCD* matrix of a $\lambda_0/4$ transmission line is

$$\begin{bmatrix} A_0 & B_0 \\ C_0 & D_0 \end{bmatrix} = \begin{bmatrix} 0 & jZ_0 \\ j\dfrac{1}{Z_0} & 0 \end{bmatrix}. \quad (7)$$

TABLE I
SPICE Parameters of an SMS7630 Diode

B_v	C_{j0}	I_s	R_s	V_{bi}
2.0 V	0.14 pF	5 μA	20 Ω	0.34 V

When $A = D = 0$, we can obtain

$$\frac{1}{Z_{CS}}\left(\frac{\cos^2\theta_{CS} - \sin^2\theta_{CS}}{\sin\theta_{CS}\cos\theta_{CS}}\right) = \frac{\tan\theta_{C1}}{Z_{C1}} + \frac{\tan\theta_{C2}}{Z_{C2}}. \quad (8)$$

We substitute B and C into the chain matrix and obtain

$$Z_0 = Z_S \tan\theta_S. \quad (9)$$

Cross circuits have characteristic impedances Z_{02} and Z_{03} at f_2 and f_3 [22]

$$Z_{02} = Z_{CS}\tan k_2\theta_{CS} \quad (10)$$
$$Z_{03} = Z_{CS}\tan k_3\theta_{CS}. \quad (11)$$

Because the admittances at f_2 and f_3 looking to the right in Plane A are G_2 and G_3, respectively, we have

$$Z_{02}^2 = \frac{Z_{\text{IN}}}{G_2}, \quad Z_{03}^2 = \frac{Z_{\text{IN}}}{G_3}. \quad (12)$$

Solving (10)–(12), we can solve for Z_{CS} and θ_{CS}. At frequency f_1, the *ABCD* matrix looking to the right from Plane A is

$$\begin{bmatrix} A_{f1} & B_{f1} \\ C_{f1} & D_{f1} \end{bmatrix} = \begin{bmatrix} A & B \\ C & D \end{bmatrix}\begin{bmatrix} 1 & 0 \\ G_{\text{IN}} & 1 \end{bmatrix} = \begin{bmatrix} A + BG_{\text{IN}} & B \\ C + DG_{\text{IN}} & D \end{bmatrix} \quad (13)$$

where $G_{\text{IN}} = 1/Z_{\text{IN}}$. Therefore, at f_1, it obtains

$$Y_1 = \frac{C_{f1}}{A_{f1}} = \frac{C + DG_{\text{IN}}}{A + BG_{\text{IN}}} = G_1 + jB_{11}. \quad (14)$$

Based on the derivation, the designed triple-band matching network can realize pure resistance impedance matching at f_2 and f_3 and complex impedance matching at f_1.

C. Design of the Octave Rectifier

The design uses an SMS7630 diode with SPICE parameters shown in Table I. First, Part A is a bandstop structure [23], which can reflect the high harmonics and adjust the impedance of the diode to simplify subsequent design. The impedance Z_a ($Z_a = 1/Y_a$) curve of the diode after series connection with Part A at different frequencies is shown in Fig. 3(a). The frequency intersecting with the real axis of the Smith chart is as f_2, $f_2 = 2.05$ GHz, $f_1 = 1.3$ GHz, and $f_3 = 2.6$ GHz. Then, determining the admittances Y_a corresponding to the f_1, f_2, and f_3, design and optimize the impedance compensation structure and matching network according to Y_a. The impedance variation curve Z ($Z = 1/Y$) of the rectifier in parallel with Part B is shown in Fig. 3(b). It is seen that the input impedance of the rectifier is zero in the imaginary part from f_2 to f_3, whereas it is negative in the frequency range of f_1 to f_2. The real parts of the rectifier input impedance at f_2 and f_3 are around 120 and 280 Ω, respectively, which are brought into (10)–(12) to obtain $Z_{CS} \approx 100$ Ω and $\theta_{cs} \approx \lambda_g/11$. After optimizing the design, the input impedance Z_{IN} of the rectifier after cascading with matching network Part C is shown in Fig. 3(c), and the rectifier is well matched with the signal source.

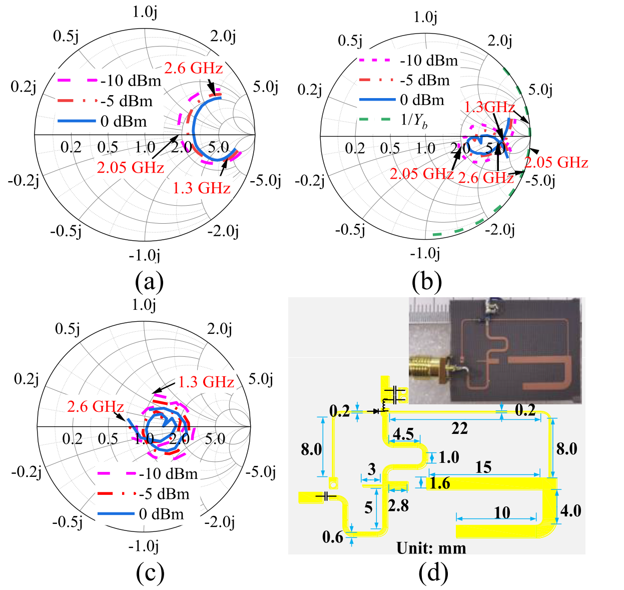

Fig. 3. (a) Z_a. (b) Z ($Z = 1/Y$). (c) Z_{IN}. (d) Layout and photograph of the proposed octave rectifier.

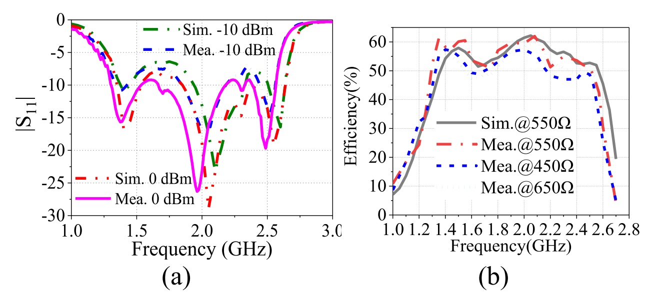

Fig. 4. (a) $|S_{11}|$ with various frequencies. (b) PCE versus frequency with different dc loads at 0 dBm.

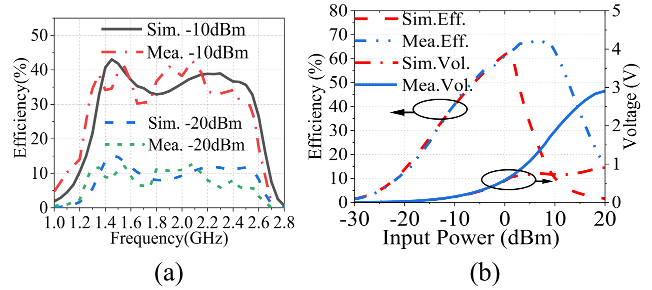

Fig. 5. (a) PCE at −10 and −20 dBm. (b) PCE versus input power at 2.08 GHz.

III. Measurement and Analysis

We designed and fabricated an octave rectifier with an operating bandwidth of 1.3–2.6 GHz and measured its rectification efficiency. F4B-2 is the substrate for the rectifier, with a relative dielectric constant of 2.65. The layout and photograph octave rectifier are illustrated in Fig. 3(d). C_1 (39 pF) is a dc-block capacitor. The dc-pass filter comprises an inductor L (22 nH) along with two capacitors, C_2 (13 pF) and C_3 (39 pF).

Fig. 4(a) displays the simulated and measured reflection coefficient $|S_{11}|$ with different frequencies at 0 and 10 dBm. The $|S_{11}|$ is less than −10 dB at 0 dBm, which is well matched. As depicted in Fig. 4(b), the conversion efficiency is simulated and measured against the frequency for an input power of 0 dBm with different dc loads. The rectifier achieves a PCE of more than 50% over 1.3–2.55 GHz with 550 Ω.

TABLE II
Comparison With Previous Rectifiers

Ref	Diode Models and Number	Bandwidth range for PCE >50%			Size (mm^2)
		Frequency range (GHz)	Relative bandwidth (%)	Power (dBm)	
[12]	BAT15-03W,1	1.77-2.88	47.7	0	23×23
[14]	HSMS286,1	2-3.3	49.1	4	31×18
[15]	SMS7630, 2	1-1.7	51.9	0	35×25
[16]	HSMS286, 1	1.5-2.85	49.0	5	37×10
[19]	SMS7630,4	1.6-3.4	66.6	8	22×24
This Work	SMS7630, 1	1.3-2.55	64.9	0	32×21

It is reaching an octave level with a relative bandwidth of 64.9%. The measurement results at lower input power levels are shown in Fig. 5(a). At −10 dBm, the rectifier has a PCE of more than 30% in the octave range of 1.25–2.5 GHz. Fig. 5(b) depicts the rectifier operating optimally at 2.08 GHz, obtaining a maximum rectification efficiency of 67.5% at 6 dBm. The higher measured efficiency at the large-power state is mainly due to the higher reverse breakdown voltage of the actual diode.

Table II displays a comparative analysis of the rectifier's performance compared with previous studies. The findings reveal that the proposed rectifier achieves a fractional bandwidth (with PCE > 50%) of 64.9%, the highest among the compared studies at 0 dBm, and it utilizes only one diode.

IV. Conclusion

In this letter, a low-power and high-efficiency octave rectifier is proposed and designed for electromagnetic energy harvesting. The design is successfully broadened by partitioning the operating frequency band of the rectifier into two segments, resistance and impedance matching, in accordance with the impedance variation. The rectifier has a more than 50% rectification efficiency between 1.3 and 2.55 GHz. The rectifier design is applicable for electromagnetic energy harvesting.

$$\begin{bmatrix} A & B \\ C & D \end{bmatrix} = \begin{bmatrix} \cos 2\theta_{CS} - \frac{1}{2} T_0 Z_{CS} \sin 2\theta_{CS} & j Z_{CS}\left(\sin 2\theta_{CS} - T_0 Z_{CS} \sin^2 \theta_{CS}\right) \\ j \frac{1}{Z_{CS}}\left(\sin 2\theta_{CS} + T_0 Z_{CS} \cos^2 \theta_{CS}\right) & \cos 2\theta_{CS} - \frac{1}{2} T_0 Z_{CS} \sin 2\theta_{CS} \end{bmatrix} \tag{5}$$

$$T_0 = \left(\frac{\tan \theta_{C1}}{Z_{C1}} + \frac{\tan \theta_{C2}}{Z_{C2}}\right) \tag{6}$$

REFERENCES

[1] N. Shinohara, "Trends in wireless power transfer: WPT technology for energy harvesting, mllimeter-wave/THz rectennas, MIMO-WPT, and advances in near-field WPT applications," *IEEE Microw. Mag.*, vol. 22, no. 1, pp. 46–59, Jan. 2021.

[2] Y. Huang, N. Shinohara, and T. Mitani, "Impedance matching in wireless power transfer," *IEEE Trans. Microw. Theory Techn.*, vol. 65, no. 2, pp. 582–590, Feb. 2017.

[3] C. Liu, H. Lin, Z. He, and Z. Chen, "Compact patch rectennas without impedance matching network for wireless power transmission," *IEEE Trans. Microw. Theory Techn.*, vol. 70, no. 5, pp. 2882–2890, May 2022.

[4] H. Lin, X. Chen, Z. He, Y. Xiao, W. Che, and C. Liu, "Wide input power range X-band rectifier with dynamic capacitive self-compensation," *IEEE Microw. Wireless Compon. Lett.*, vol. 31, no. 5, pp. 525–528, May 2021.

[5] P. Kamalinejad, C. Mahapatra, Z. Sheng, S. Mirabbasi, V. C. M. Leung, and Y. L. Guan, "Wireless energy harvesting for the Internet of Things," *IEEE Commun. Mag.*, vol. 53, no. 6, pp. 102–108, Jun. 2015.

[6] P. Wu, S.-P. Gao, Y.-D. Chen, Z. H. Ren, P. Yu, and Y. Guo, "Harmonic-based integrated rectifier-transmitter for uncompromised harvesting and low-power uplink," *IEEE Trans. Microw. Theory Techn.*, vol. 71, no. 2, pp. 870–880, Feb. 2023.

[7] S. Kim et al., "Ambient RF energy-harvesting technologies for self-sustainable standalone wireless sensor platforms," *Proc. IEEE*, vol. 102, no. 11, pp. 1649–1666, Nov. 2014.

[8] G. C. Martins and W. A. Serdijn, "An RF energy harvesting and power management unit operating over -24 to $+15$ dBm input range," *IEEE Trans. Circuits Syst. I, Reg. Papers*, vol. 68, no. 3, pp. 1342–1353, Mar. 2021.

[9] J. Kimionis, A. Collado, M. M. Tentzeris, and A. Georgiadis, "Octave and decade printed UWB rectifiers based on nonuniform transmission lines for energy harvesting," *IEEE Trans. Microw. Theory Techn.*, vol. 65, no. 11, pp. 4326–4334, Nov. 2017.

[10] P. Wu et al., "Compact high-efficiency wideband rectifier with multistage-transmission-line matching," *IEEE Trans. Circuits Syst. II, Exp. Lett.*, vol. 66, no. 8, pp. 1316–1320, Aug. 2019.

[11] D.-A. Nguyen and C. Seo, "Design of high-efficiency broadband rectifier with harmonic control for wireless power transfer and energy harvesting," *IEEE Microw. Wireless Compon. Lett.*, vol. 32, no. 10, pp. 1231–1234, Oct. 2022.

[12] G. T. Bui, D.-A. Nguyen, and C. Seo, "A highly efficient design of broadband rectifier with harmonic suppression transferring for energy harvesting and wireless power transfer," *IEEE Microw. Wireless Compon. Lett.*, vol. 33, no. 7, pp. 1059–1062, Jul. 2023.

[13] S. F. Bo, J.-H. Ou, and X. Y. Zhang, "Ultrawideband rectifier with extended dynamic-power-range based on wideband impedance compression network," *IEEE Trans. Microw. Theory Techn.*, vol. 70, no. 8, pp. 4026–4035, Aug. 2022.

[14] Z. He and C. Liu, "A compact high-efficiency broadband rectifier with a wide dynamic range of input power for energy harvesting," *IEEE Microw. Wireless Compon. Lett.*, vol. 30, no. 4, pp. 433–436, Apr. 2020.

[15] W. Liu, K. Huang, T. Wang, J. Hou, and Z. Zhang, "Broadband high-efficiency RF rectifier with a cross-shaped match stub of two one-eighth-wavelength transmission lines," *IEEE Microw. Wireless Compon. Lett.*, vol. 31, no. 10, pp. 1170–1173, Oct. 2021.

[16] H. He, H. Lin, P. Wu, Q. Li, and C. Liu, "Compact high-efficiency wideband rectifier based on coupled transmission line," *IEEE Trans. Circuits Syst. II, Exp. Lett.*, vol. 69, no. 11, pp. 4404–4408, Nov. 2022.

[17] H. S. Park and S. K. Hong, "Broadband RF-to-DC rectifier with uncomplicated matching network," *IEEE Microw. Wireless Compon. Lett.*, vol. 30, no. 1, pp. 43–46, Jan. 2020.

[18] W. Liu, K. Huang, T. Wang, J. Hou, and Z. Zhang, "A compact high-efficiency RF rectifier with widen bandwidth," *IEEE Microw. Wireless Compon. Lett.*, vol. 32, no. 1, pp. 84–87, Jan. 2022.

[19] W. Liu, K. Huang, T. Wang, J. Hou, and Z. Zhang, "A compact ultra-broadband RF rectifier using Dickson charge pump," *IEEE Microw. Wireless Compon. Lett.*, vol. 32, no. 6, pp. 591–594, Jun. 2022.

[20] H. Long, F. Cheng, S. Yu, C. Gu, and K. Huang, "High-efficiency broadband rectifier with compact size for wireless power transfer," *Microw. Opt. Technol. Lett.*, vol. 64, no. 11, pp. 2007–2013, Nov. 2022.

[21] S. Zheng, W. Liu, and Y. Pan, "Design of an ultra-wideband high-efficiency rectifier for wireless power transmission and harvesting applications," *IEEE Trans. Ind. Informat.*, vol. 15, no. 6, pp. 3334–3342, Jun. 2019.

[22] Z. Hu, C. Huang, S. He, and F. You, "Tri-band matching technique based on characteristic impedance transformers for concurrent tri-band power amplifiers design," in *Proc. IEEE Region Conf.*, Nov. 2015, pp. 1–3.

[23] C. Liu, F. Tan, H. Zhang, and Q. He, "A novel single-diode microwave rectifier with a series band-stop structure," *IEEE Trans. Microw. Theory Techn.*, vol. 65, no. 2, pp. 600–606, Feb. 2017.